

Real-world Image Dehazing with Coherence-based Label Generator and Cooperative Unfolding Network

Chengyu Fang^{1,*}, Chunming He^{1,2*}, Fengyang Xiao³, Yulun Zhang^{4,†},
Longxiang Tang¹, Yuelin Zhang⁵, Kai Li⁶, Xiu Li^{1,†}

¹Shenzhen International Graduate School, Tsinghua University, ²Duke University,

³Sun Yat-sen University, ⁴Shanghai Jiao Tong University,

⁵The Chinese University of Hong Kong, ⁶Meta Reality Labs

Abstract

Real-world Image Dehazing (RID) aims to alleviate haze-induced degradation in real-world settings. This task remains challenging due to the complexities in accurately modeling real haze distributions and the scarcity of paired real-world data. To address these challenges, we first introduce a cooperative unfolding network that jointly models atmospheric scattering and image scenes, effectively integrating physical knowledge into deep networks to restore haze-contaminated details. Additionally, we propose the first RID-oriented iterative mean-teacher framework, termed the Coherence-based Label Generator, to generate high-quality pseudo labels for network training. Specifically, we provide an optimal label pool to store the best pseudo-labels during network training, leveraging both global and local coherence to select high-quality candidates and assign weights to prioritize haze-free regions. We verify the effectiveness of our method, with experiments demonstrating that it achieves state-of-the-art performance on RID tasks. Code will be available at <https://github.com/cnyvfang/CORUN-Colaborator>.

1 Introduction

Real-world image dehazing (RID) is a challenging task that aims to restore images affected by complex haze in real-world scenarios. The goal is to generate visual-appealing results while enhancing the performance of downstream tasks [15, 46]. The atmospheric scattering model (ASM), providing a physical framework for real-world dehazing, is formulated as follows:

$$P(x) = J(x)t(x) + A(1 - t(x)), \quad (1)$$

where $P(x)$ and $J(x)$ are the hazy image and the haze-free counterpart. A signifies the global atmospheric light. $t(x)$ characterizes the transmission map reflecting varying degrees of haze visibility across different regions.

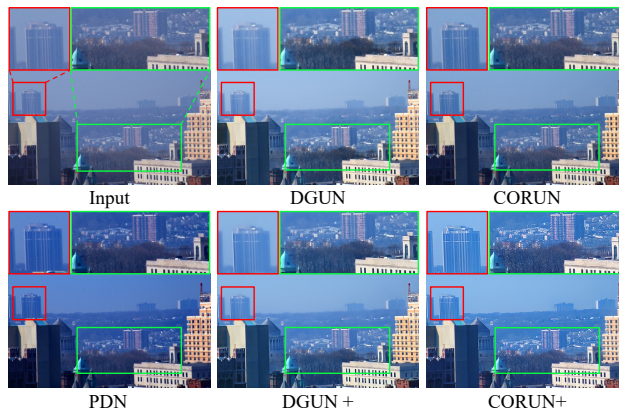


Figure 1: Results of cutting-edge methods. Our CORUN better restores hazy-contaminated details. Furthermore, techniques optimized by our Colaborator framework, indicated by a "+" suffix, exhibit strong generalization in haze removal and color correction.

*Equal Contribution, † Corresponding Author

Conventional methods [20, 24] are limited by fixed feature extractors, which struggle to handle the complexities of real haze. Although existing deep learning-based methods [37, 54] demonstrate improved performance, they face two significant challenges: (1) These methods do not accurately model the complex distribution of haze, leading to color distortion (as illustrated in fig. 1 DGUN [37]). (2) Real-world settings lack sufficient paired data for network training while optimizing the network with synthesized data brings a domain gap, limiting the generalizability of the models.

To overcome the first challenge, PDN [57] first introduces unfolding network [16, 56] to the RID field. In specific, PDN unfolds the iterative optimization steps of an ASM-based solution into a deep network for end-to-end training, incorporating physical information into the deep network. However, PDN does not effectively leverage the complementary information between the dehazed image and the transmission map, bringing overfitting problems and resulting in detail blurring (see fig. 1).

In this paper, we introduce the COopeRative Unfolding Network (CORUN), also derived from the ASM-based function, to address PDN’s limitations and better model real hazy distribution. CORUN cooperatively models the atmospheric scattering and image scene by incorporating Transmission and Scene Gradient Descent Modules at each stage, corresponding to each iteration of the traditional optimization algorithm. To prevent overfitting, we introduce a global coherence loss, which constrains the entire pipeline to adhere to physical laws while alleviating constraints on the intermediate layers. These design choices collectively ensure that CORUN effectively integrates physical information into deep networks, thereby excelling in restoring haze-contaminated details, as depicted in fig. 1.

To enhance generalizability in real-world scenarios, we introduce the first RID-oriented iterative mean-teacher framework, named Coherence-based label generator (Colabator), designed to generate high-quality dehazed images as pseudo labels for training dehazing methods. Specifically, Colabator employs a teacher network, a dehazing network pretrained on synthesized datasets, to generate dehazed images on label-free real-world datasets. These restored images are stored in a dynamically updated label pool as pseudo labels for training the student network, which shares the same structure as the teacher network but with distinct weights. During network training, the teacher network generates multiple pseudo labels for a single real-world hazy image. We propose selecting the best labels to store in the label pool based on visual fidelity and dehazing performance.

To achieve this, we design a compound image quality assessment strategy tailored to the dehazing task, evaluating the global coherence of the dehazed images and selecting the most visually appealing ones without distortions for inclusion in the label pool. Additionally, we propose a patch-level certainty map to encourage the network to focus on well-restored regions of the dehazed pseudo labels, effectively constraining the local coherence between the outputs of the student model and the teacher model. As shown in fig. 1, Colabator, generating high-quality pseudo labels for network training, enhances the student dehazing network’s capacity for haze removal and color correction.

Our contributions are summarized as follows:

- (1) We propose a novel dehazing method, CORUN, to cooperatively model the atmospheric scattering and image scene, effectively integrating physical information into deep networks.
- (2) We propose the first iterative mean-teacher framework, Colabator, to generate high-quality pseudo labels for network training, enhancing the network’s generalization in haze removal.
- (3) We evaluate our CORUN with the Colabator framework on real-world dehazing tasks. Abundant experiments demonstrate that our method achieves state-of-the-art performance.

2 Related Works

2.1 Real-world Image Dehazing

The dissonance between synthetic and real haze distributions often hinders existing Learning-based dehazing methods [10, 13, 31, 42, 60] from effectively dehazing real-world images. Consequently, there’s a growing emphasis on tackling challenges specific to real-world dehazing [6, 43, 67, 53, 64].

Given the characteristics of real haze, RIDCP [54] and Wang *et al.* [52] proposed novel haze synthesis pipelines. However, relying solely on synthetic data limits models’ robustness in real-world dehazing scenarios. Recognizing the distributional disparities between synthetic and real haze, methods like CDD-GAN [5], D4 [59], Shao *et al.* [47], and Li *et al.* [30] have utilized CycleGAN [69] for dehazing.

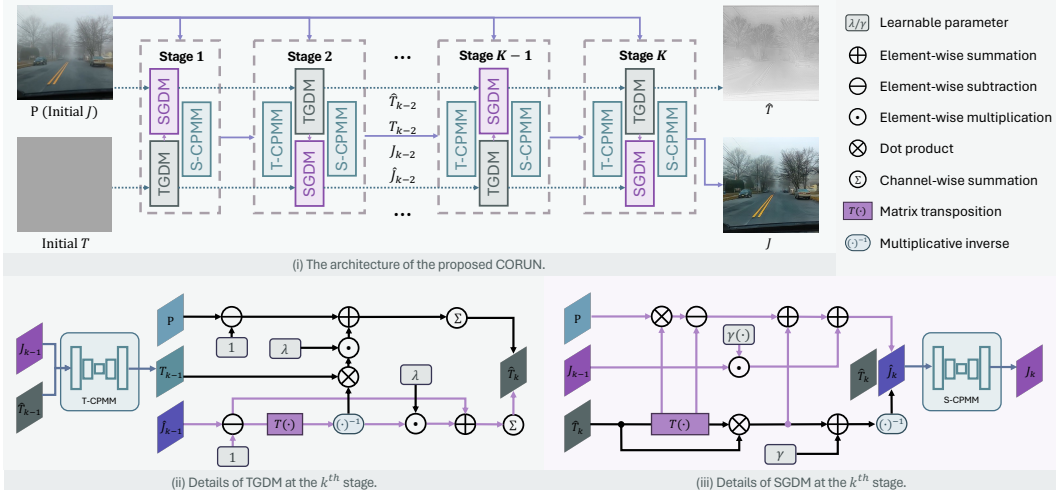


Figure 2: The architecture of the proposed CORUN with the detailed at k^{th} stage.

Despite this, the challenges inherent in GAN [12] training often result in artifacts. Some approaches combine synthetic and real-world data, applying unsupervised loss to supervise real-world dehazing learning [6]. However, these losses lack sufficient precision, leading to suboptimal results. Other methods leverage pseudo-labels [32, 8, 50], but the erroneous pseudo-labels cause degrade quality.

To address these challenges, we introduce a coherence-based pseudo labeling method termed Colaborator. Our approach selectively identifies and prioritizes high-quality regions within pseudo labels, leading to enhanced robustness and superior generation quality for real-world image dehazing.

2.2 Deep Unfolding Image Restoration

Deep Unfolding Networks (DUNs) integrate model-based and learning-based approaches [22, 23] and thus offer enhanced interpretability and flexibility compared to traditional learning-based methods. Increasingly, DUNs are being utilized for various image tasks, including image super-resolution [63], compressive sensing [61, 62], hyperspectral image reconstruction [28], and image fusion [68]. DGUN [37] proposes a general form of proximal gradient descent to learn degradation. However, it fails to decouple prior knowledge, relying solely on single-path DUN to model degradation and construct mappings, posing challenges in comprehending complex degradation. Yang and Sun first introduced DUNs to the image dehazing field and proposed PDN [57]. However, PDN does not exploit the complementary information between the dehazed image and the transmission map, resulting in detail blurring. Our CORUN optimizes the atmospheric scattering model and the image scene feature through dual proximal gradient descent, thus preventing overfitting and facilitating detail restoration.

3 Methodology

3.1 Cooperative Unfolding Network

We propose the Cooperative Unfolding Network (CORUN), the first Deep Unfolding Network (DUN) method utilizing Proximal Gradient Descent (PGD) to optimize image dehazing performance. CORUN leverages the Atmospheric Scattering Model (ASM) and neural image reconstruction in a cooperative manner. Each stage of CORUN includes Transmission and Scene Gradient Descent Modules (T&SGDM) paired with Cooperative Proximal Mapping Modules (T&S-CPMM). These modules work together to model atmospheric scattering and image scene features, enabling the adaptive capture and restoration of global composite features within the scene.

According to eq. (1), given a hazy image $\mathbf{P} \in \mathbb{R}^{H \times W \times 3}$, we initialize a transmission map $\mathbf{T} \in \mathbb{R}^{H \times W \times 1}$. In gradient descent, we simplify the atmospheric light $A \in \mathbb{R}^3$ and implicitly estimate it in the CORUN pipeline to focus on the detailed characterization of the scene and the relationship between volumetric haze and scene. Hence, eq. (1) can be rewrite as

$$\mathbf{P} = \mathbf{J} \cdot \mathbf{T} + \mathbf{I} - \mathbf{T}, \quad (2)$$

Where \mathbf{J} means the clear image without hazy, \mathbf{I} is the all-one matrix. Based on eq. (2), we can define our cooperative dehazing energy function like

$$L(\mathbf{J}, \mathbf{T}) = \frac{1}{2} \|\mathbf{P} - \mathbf{J} \cdot \mathbf{T} + \mathbf{T} - \mathbf{I}\|_2^2 + \psi(\mathbf{J}) + \phi(\mathbf{T}), \quad (3)$$

where $\psi(\mathbf{J})$ and $\phi(\mathbf{T})$ are regularization terms on \mathbf{T} and \mathbf{J} . We introduce two auxiliary variables $\hat{\mathbf{T}}$ and $\hat{\mathbf{J}}$ to approximate \mathbf{T} and \mathbf{J} , respectively. This leads to the following minimization problem:

$$\{\hat{\mathbf{J}}, \hat{\mathbf{T}}\} = \arg \min_{\mathbf{J}, \mathbf{T}} L(\mathbf{J}, \mathbf{T}). \quad (4)$$

Transmission optimization. Give the estimated coarse transmission map \mathbf{T} and dehazed image $\hat{\mathbf{J}}_{k-1}$ at iteration $k-1$, the variable \mathbf{T} can be updated as:

$$\mathbf{T}_k = \arg \min_{\mathbf{T}} \frac{1}{2} \sum_{c \in \{R, G, B\}} \left\| \mathbf{P}^c - \hat{\mathbf{J}}_{k-1}^c \cdot \mathbf{T} + \mathbf{T} - \mathbf{I} \right\|_2^2 + \phi(\mathbf{T}). \quad (5)$$

We construct the proximal mapping between $\hat{\mathbf{T}}$ and \mathbf{T} by a encoder-decoder like neural network which we named T-CPMM and denoted as prox_ϕ :

$$\mathbf{T}_k = \text{prox}_\phi(\mathbf{J}_{k-1}, \hat{\mathbf{T}}_k), \quad (6)$$

the auxiliary variables $\hat{\mathbf{T}}$, which we calculate by our proposed TGDM can be formulated as:

$$\hat{\mathbf{T}}_k = \sum_{c \in \{R, G, B\}} \left(\mathbf{I} - \hat{\mathbf{J}}_{k-1}^c + \frac{\lambda_k}{(\mathbf{I} - \hat{\mathbf{J}}_{k-1}^c)^\top} \right)^{-1} \cdot \left(\mathbf{I} - \mathbf{P}^c \frac{\lambda_k \mathbf{T}_{k-1}}{(\mathbf{I} - \hat{\mathbf{J}}_{k-1}^c)^\top} \right). \quad (7)$$

The variable λ_k is a learnable parameter, we enable CORUN to learn this parameter at each stage during the end-to-end learning process, allowing the network to adaptively control the updates in iteration.

Scene optimization. Give $\hat{\mathbf{T}}_k$ and \mathbf{J} , the variable \mathbf{J} can be updated as:

$$\mathbf{J}_k = \arg \min_{\mathbf{J}} \frac{1}{2} \|\mathbf{P} - \mathbf{J} \cdot \hat{\mathbf{T}}_k + \hat{\mathbf{T}}_k - \mathbf{I}\|_2^2 + \psi(\mathbf{J}). \quad (8)$$

Same as the proximal mapping process in the transmission optimization, S-CPMM has the similar structure as T-CPMM but different inputs, we denote S-CPMM as prox_ψ :

$$\mathbf{J}_k = \text{prox}_\psi(\hat{\mathbf{J}}_k, \hat{\mathbf{T}}_k), \quad (9)$$

where the $\hat{\mathbf{J}}_k$ we process by our SGDM can be presented as:

$$\hat{\mathbf{J}}_k = (\hat{\mathbf{T}}_k^\top \hat{\mathbf{T}}_k + \mu_k \mathbf{I})^{-1} \cdot (\hat{\mathbf{T}}_k^\top \mathbf{P} + \hat{\mathbf{T}}_k^\top \hat{\mathbf{T}}_k - \hat{\mathbf{T}}_k^\top + \mu_k \mathbf{J}_{k-1}), \quad (10)$$

as the λ_k in transmission optimization, μ_k is also a learnable parameter to bring more generalization capabilities to the network.

Details about CPMM. T-CPMM and S-CPMM share the same structure, which is modified from MST [2] for improved mapping quality. Each CPMM block uses a 4-channel convolution to embed \mathbf{T} and \mathbf{J} into a 30-dimensional feature map. The distinction between T-CPMM and S-CPMM lies in their outputs: T-CPMM produces a 1-channel result to aid TGDM in predicting a scene-compliant transmission map, whereas S-CPMM generates a 3-channel RGB image. This enables S-CPMM to learn additional scene feature information, such as atmospheric light and blur, assisting SGDM in generating higher-quality dehazed results with more details. For more efficient computation, each CPMM comprises only 3 layers with [1, 1, 1] blocks, doubling the dimensions with increasing depth.

3.2 Coherence-based Pseudo Labeling by Colaborator

We generate and select pseudo labels using our proposed plug-and-play coherence-based label generator, Colaborator. Colaborator consists of a teacher network with weights θ_{tea} shared with the student network θ_{stu} via exponential moving average (EMA). It employs a tailored mean-teacher strategy with a trust weighting process and an optimal label pool to generate high-quality pseudo labels, addressing the scarcity of real-world data. Figure 3 illustrates the pipeline of our Colaborator.

Iterative mean-teacher dehazing. Given a real hazy image $\mathbf{P}_{LQ}^R \in \mathbb{R}^{H \times W \times 3}$, we initially apply augmentations to generate corresponding strongly degraded data using a strong augmentor $\mathcal{A}_s(\cdot)$,

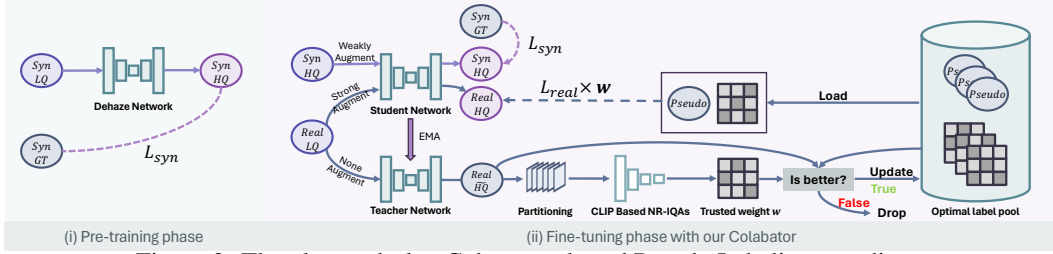


Figure 3: The plug-and-play Coherence-based Pseudo Labeling paradigm.

which randomly applies adjustments such as contrast, brightness, posterize, sharpness, JPEG compression, and Gaussian blur. Unlike the common mean-teacher strategy, we omit functions like solarize, equalize, shear, and translate to prevent unnecessary degradation that might mislead model learning. We use the non-augmented image as the input for the teacher network and the strongly augmented image for the student network, generating the following results:

$$\mathbf{P}_{HQ}^R, \mathbf{T}_{HQ}^R = f_{\theta_{tea}}(\mathbf{P}_{LQ}^R), \quad \mathbf{P}_{HQ}^R, \mathbf{T}_{HQ}^R = f_{\theta_{stu}}(\mathcal{A}_s(\mathbf{P}_{LQ}^R)), \quad (11)$$

where $\mathbf{P}_{HQ}^R \in \mathbb{R}^{H \times W \times 3}$ is the result from the teacher network using the non-augmented input, and $\mathbf{P}_{HQ}^R \in \mathbb{R}^{H \times W \times 3}$ represents the result from the student network by strong augment input and $\mathbf{T}_{HQ}^R, \mathbf{T}_{HQ}^R$ are the corresponding transmission map. The different degrees of data augmentation lead to varying dehazing results, typically resulting in \mathbf{P}_{HQ}^R having better quality than \mathbf{P}_{HQ}^R . This approach ensures the model descends in the correct direction and helps mitigate the overfitting issues often associated with direct pseudo-label learning methods. By iterating, our teacher network generates increasingly high-quality pseudo-labels, providing more reliable supervision for model learning.

Label trust weighting. To better leverage the pseudo-dehazed images \mathbf{P}_{HQ}^R generated by the teacher network for model supervision, we designed a composite image quality assessment strategy for further processing these pseudo-dehazed images and get the trusted weight w which means the reliability of each location of an image. Our composite strategy primarily consists of a haze density evaluator $\mathcal{D}(\cdot)$ based on pre-trained CLIP [44] model and fixed text feature, and a non-reference image quality evaluator $\mathcal{Q}(\cdot)$. We partition \mathbf{P}_{HQ}^R into an sequence $\mathbf{S}_{HQ}^R \in \mathbb{R}^{N \times N \times 3 \times (H/N) \times (W/N)}$ and use $\mathcal{D}(\cdot)$ and $\mathcal{Q}(\cdot)$ to predict the density score and quality score. The final trusted weight w we can get from:

$$w = \Psi(\text{norm}(\mathcal{D}(\mathbf{S}_{HQ}^R)) + \text{norm}(\mathcal{Q}(\mathbf{S}_{HQ}^R))), \quad (12)$$

where Ψ is compose sequence to map and resize as \mathbf{P}_{HQ}^R , $\text{norm}(\cdot)$ means normalize scores from 0 to 1, that higher score means lower haze density and better image quality.

Optimal label pool. To ensure the use of optimal pseudo-labels and avoid domain adaptation collapse due to instability during training, we proposed an optimal label pool \mathcal{P} to maintain the pseudo-labels in their optimal state. The overall procedure of our optimal label pool process is summarized in algorithm 1, compare pseudo-dehazed image $\mathbf{P}_{HQ_i}^R$ with previous pseudo-label $\mathbf{P}_{Pse_i}^R$ and update pseudo-dehazed image as pseudo-label if it better than previous. To summarize the algorithm 1 and eq. (11), the overall process of Colaborator can be formalize as:

$$\mathbf{P}_{HQ}^R, \mathbf{T}_{HQ}^R, \mathbf{P}_{Pse}^R, \mathbf{T}_{Pse}^R, w_{pse} = \mathcal{C}(\mathbf{P}_{LQ}^R, \theta_{tea}, \theta_{stu}, \mathcal{A}_s, \mathcal{D}(\cdot), \mathcal{Q}(\cdot), \mathcal{P}), \quad (13)$$

where \mathcal{C} is our Colaborator framework, \mathbf{P}_{Pse}^R is the paired pseudo label of $\mathcal{A}_s(\mathbf{P}_{LQ}^R)$, \mathbf{T}_{Pse}^R is the corresponding pseudo transmission map, w_{pse} means the trusted weight of the pseudo label.

Weights update. The teacher network's weights θ_{tea} are updated by exponential moving average (EMA) of the student network's weights θ_{stu} , which is denoted as follows:

$$\theta_{tea} = \eta\theta_{tea} + (1 - \eta)\theta_{stu}, \quad (14)$$

where η is momentum and $\eta \in (0, 1)$. Using this update strategy, the teacher model can aggregate previously learned weights immediately after each training step, ensuring updating stability.

3.3 Semi-supervised Real-world Image Dehazing

To achieve success in real-world dehazing, we designed several loss functions for our CORUN and Colaborator to constrain their learning process. We introduce a reconstruction loss using the L_1 norm

Algorithm 1 Optimal label pool process

Require: Haze density evaluator $\mathcal{D}(\cdot)$ and image quality evaluator $\mathcal{Q}(\cdot)$;
Optimal label pool \mathcal{P} ;
Sample a batch of real hazy images $\{\mathbf{P}_{LQ_i}^R\}_{i=1}^b$;
for each $\mathbf{P}_{LQ_i}^R$ **do**
 Get teacher network prediction: $\mathbf{P}_{\widehat{H}Q_i}^R, \mathbf{T}_{\widehat{H}Q_i}^R = f_{\theta_{tea}}(\mathbf{P}_{LQ_i}^R)$;
 Partition $\mathbf{P}_{\widehat{H}Q_i}^R$ into $N \times N$ and get $\mathbf{S}_{\widehat{H}Q_i}^R$;
 Compute score map of $\mathbf{S}_{\widehat{H}Q_i}^R$: $d_i = \text{norm}(\mathcal{D}(\mathbf{S}_{\widehat{H}Q_i}^R))$, and $q_i = \text{norm}(\mathcal{Q}(\mathbf{S}_{\widehat{H}Q_i}^R))$;
 Load $\mathbf{P}_{Psei}^R, \mathbf{T}_{Psei}^R, w_{Psei}, d_{Psei}, q_{Psei} = \mathcal{P}(i)$
 if $d_i > d_{Psei}$ and $q_i > q_{Psei}$ **then**
 Compute trusted weight: $w_i = \Psi(d_i + q_i)$
 Update $\mathcal{P}(i) = (\mathbf{P}_{\widehat{H}Q_i}^R, \mathbf{T}_{\widehat{H}Q_i}^R, w_i, d_i, q_i)$
 Return $\mathbf{P}_{\widehat{H}Q_i}^R, \mathbf{T}_{\widehat{H}Q_i}^R, w_i$ as pseudo label.
 else
 Return $\mathbf{P}_{Psei}^R, \mathbf{T}_{Psei}^R, w_{Psei}$ as pseudo label.
 end if
end for

$\|\cdot\|_1$. To enhance visual perception, we employ contrastive and common perceptual regularization to ensure the consistency of the reconstruction results with the ground truth in terms of features at different levels. The perceptual loss is defined as follows:

$$L_{Rec}^{common}(\mathbf{P}_{HQ}, \mathbf{P}_{GT}) = \|\mathbf{P}_{GT}, \mathbf{P}_{HQ}\|_1 + \beta_c \sum_{i=1}^n \tau_i \|\varphi_i(\mathbf{P}_{GT}), \varphi_i(\mathbf{P}_{HQ})\|_1, \quad (15)$$
$$L_{Rec}^{contra}(\mathbf{P}_{LQ}, \mathbf{P}_{HQ}, \mathbf{P}_{GT}) = \|\mathbf{P}_{GT}, \mathbf{P}_{HQ}\|_1 + \beta_c \sum_{i=1}^n \tau_i \frac{\|\varphi_i(\mathbf{P}_{GT}), \varphi_i(\mathbf{P}_{HQ})\|_1}{\|\varphi_i(\mathbf{P}_{LQ}), \varphi_i(\mathbf{P}_{HQ})\|_1},$$

where \mathbf{P}_{HQ} is the dehazed result, $\varphi_i(\cdot)$ means the i_{th} hidden layer of pre-trained VGG-19 [48], τ_i is the weight coefficient. Besides, to constrain the entire pipeline to obey physical laws while alleviating constraints on the intermediate layers, and prevent overfitting, we introduce a global coherence loss:

$$L_{Coh}(\mathbf{P}_{LQ}, \mathbf{P}_{HQ}, \mathbf{T}_{HQ}) = \|(\mathbf{P}_{HQ} \odot \mathbf{T}_{HQ} + (\mathbf{I} - \mathbf{T}_{HQ})) - \mathbf{P}_{LQ}\|_1, \quad (16)$$

where \odot is the Hadamard product, \mathbf{I} means the all-ones matrix as the same size of \mathbf{P}_{LQ}^S . The global coherence loss ensures that CORUN can more efficiently integrate physical information into the deep network to facilitate the recovery of more physically consistent details. In addition, we introduce a density loss L_{dens} based on $\mathcal{D}(\cdot)$ to score and constraint the model to dehaze in the semantic domain:

$$L_{Dens}(\mathbf{P}) = \mathcal{D}(\mathbf{P}). \quad (17)$$

Pre-training phase. To ensure the capacity in dehazing and transmission map estimation, we pre-trained CORUN on synthetic paired datasets which contained clear image $\mathbf{P}_{GT}^S \in \mathbb{R}^{H \times W \times 3}$ and synthetic hazy image $\mathbf{P}_{LQ}^S \in \mathbb{R}^{H \times W \times 3}$. Setting \mathbf{P}_{LQ}^S as input, we can get the result by

$$\mathbf{P}_{HQ}^S, \mathbf{T}_{HQ}^S = f_{\theta_{stu}}(\mathcal{A}_w(\mathbf{P}_{LQ}^S)), \quad (18)$$

where \mathcal{A}_w means weakly geometric data augment, \mathbf{P}_{HQ}^S means the dehazed result of synthetic hazy image, and \mathbf{T}_{HQ}^S is the corresponding transmission map. In the pre-training phase, our CORUN is optimized end-to-end using two supervised loss functions. The overall loss of the pre-training phase:

$$L_{pre} = \rho_r L_{Rec}^{contra}(\mathcal{A}_w(\mathbf{P}_{LQ}^S), \mathbf{P}_{HQ}^S, \mathbf{P}_{GT}^S) + \rho_c L_{Coh}(\mathcal{A}_w(\mathbf{P}_{LQ}^S), \mathbf{P}_{HQ}^S, \mathbf{T}_{HQ}^S) + L_{Dens}(\mathbf{P}_{HQ}^S), \quad (19)$$

where ρ_r is the trade-off weight of L_{Rec}^{contra} , ρ_c is the trade-off weight of L_{Coh} .

Fine-tuning phase. In fine-tuning phase, we adapt our CORUN pre-trained on synthetic data to the real-world domain by our Colabator framework. For more steady learning, in this phase, we train

| Metrics | Hazy | PDN [57] | MBDN [10] | DH [13] | DAD [47] | PSD [6] | D4 [59] | RIDCP [54] | DGUN [37] | Ours |
|----------|--------|--------------|-----------|---------|----------|---------|---------|---------------|-----------|---------------|
| FADE↓ | 2.484 | 0.876 | 1.363 | 1.895 | 1.130 | 0.920 | 1.358 | 0.944 | 1.111 | 0.751 |
| BRISQUE↓ | 36.642 | 30.811 | 27.672 | 33.862 | 32.241 | 27.713 | 33.210 | 17.293 | 27.968 | 11.956 |
| NIMA↑ | 4.483 | 4.464 | 4.529 | 4.522 | 4.312 | 4.598 | 4.484 | 4.965 | 4.653 | 5.315 |

Table 1: Quantitative results on RTTS dataset. **Red** and **blue** indicate the best and the second best.



Figure 4: Visual comparison on RTTS[27]. Please zoom in for a better view.

with both synthetic and real-world data. As eq. (13), we generate $\mathbf{P}_{HQ}^R, \mathbf{T}_{HQ}^R, \mathbf{P}_{Pse}^R, \mathbf{T}_{Pse}^R, w_{pse}$ from \mathbf{P}_{LQ}^R , and we get $\mathbf{P}_{HQ}^S, \mathbf{T}_{HQ}^S$ use the eq. (18). The overall loss of the fine-tuning phase:

$$\begin{aligned}
 L_{fine} = & w\rho_r L_{Rec}^{contra}(\mathcal{A}_s(\mathbf{P}_{LQ}^R), \mathbf{P}_{HQ}^R, \mathbf{P}_{Pse}^R) + \rho_r L_{Rec}^{common}(\mathbf{P}_{HQ}^S, \mathbf{P}_{GT}^S) \\
 & + w\rho_c L_{Coh}(\mathcal{A}_s(\mathbf{P}_{LQ}^R), \mathbf{P}_{HQ}^R, \mathbf{T}_{HQ}^R) + L_{Dens}(\mathbf{P}_{HQ}^S) + wL_{Dens}(\mathbf{P}_{HQ}^R).
 \end{aligned} \quad (20)$$

4 Experiments

4.1 Experimental Setup

Data Preparation. We use RIDCP500 [54] dataset, comprising 500 clear images with depth maps estimated by [21], and follow the same way of RIDCP [54] for generating paired data. During the fine-tuning phase, we incorporate the URHI subset of RESIDE dataset [27], which only consists of 4,807 real hazy images, for generating pseudo-labels and fine-tuning the network. We evaluate our framework qualitatively and quantitatively on the RTTS subset, which comprises over 4,000 real hazy images featuring diverse scenes, resolutions, and degradation. Fattal’s dataset [11], comprising 31 classic real hazy cases, serves as a supplementary source for cross-dataset visual comparison.

Implementation Details. Our framework is implemented using PyTorch [38] and trained on four NVIDIA RTX 4090 GPUs. During the pre-training phase, we train the network for 30K iterations, optimizing it with AdamW [34, 9] using momentum parameters ($\beta_1 = 0.9, \beta_2 = 0.999$) and an initial learning rate of 2×10^{-4} , gradually reduced to 1×10^{-6} with cosine annealing [33]. In Colabator, the initial learning rate is set to 5×10^{-5} with only 5K iterations. Following [54], we employ random crop and flip for synthetic data augmentation. We use DA-CLIP [35] as our haze density evaluator and MUSIQ [25] as the image quality evaluator. Our CORUN consists of 4 stages and the trade-off parameters in the loss are set to β_c, ρ_r, ρ_c are set to 0.2, 5, 10^{-2} , respectively.

Metrics. We utilize the Fog Aware Density Evaluator (FADE) [7] to assess the haze density in various methods. However, FADE focuses on haze density exclusively, overlooking other crucial

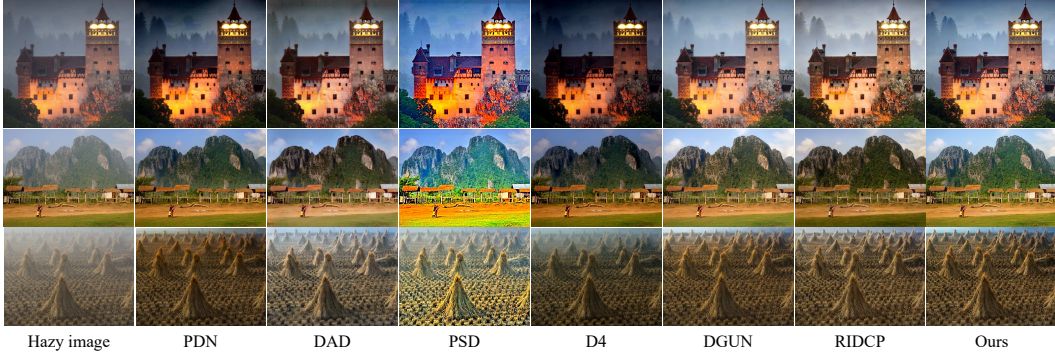


Figure 5: Visual comparison on Fattal’s data[11].

| Datasets | Metrics | w/o Colabator DGUN | w/ Colabator DGUN | w/o Colabator CORUN | w/ Colabator CORUN (Ours) |
|----------|----------|-----------------------|----------------------|------------------------|------------------------------|
| RTTS | FADE↓ | 1.111 | 0.857 | 1.091 | 0.751 |
| | BRISQUE↓ | 25.085 | 20.731 | 16.541 | 11.956 |
| | NIMA↑ | 4.813 | 5.190 | 4.856 | 5.315 |

Table 2: Generalization and Effect of our Colabator.

| Datasets | Metrics | w/o IMD | w/o Trusted weight | w/o Optimal label pool | Datasets | Metrics | Stages | | | |
|----------|----------|------------|-----------------------|---------------------------|----------|----------|--------|--------|----------|--------|
| | | | | | | | 1 | 2 | 4 (Ours) | 6 |
| RTTS | FADE↓ | 1.078 | 0.827 | 0.846 | RTTS | FADE↓ | 0.785 | 0.808 | 0.751 | 0.839 |
| | BRISQUE↓ | 16.646 | 16.606 | 15.707 | | BRISQUE↓ | 15.520 | 15.151 | 11.956 | 16.227 |
| | NIMA↑ | 4.868 | 4.867 | 5.285 | | NIMA↑ | 5.228 | 5.281 | 5.315 | 5.187 |

Table 3: Module’s Effect of our Colabator.

Table 4: Effect of stage number.

image characteristics such as color, brightness, and detail. To address this limitation, we also employ Blind/Referenceless Image Spatial Quality Evaluator (BRISQUE) [36], and Neural Image Assessment(NIMA) [49] for a more comprehensive evaluation of image quality and aesthetic. Higher NIMA scores, along with lower FADE and BRISQUE scores, indicate better performance. We use PyIQA [3] for BRISQUE and NIMA calculations, and the official MATLAB code for FADE calculations. All of these metrics are non-reference because there is no ground-truth in RTTS [27].

4.2 Comparative Evaluation

We compare our method with 8 state-of-the-art methods: PDN [57], MBDN [10], DH [13], DAD [47], PSD [6], D4 [59], RIDCP [54], DGUN [37]. The quantitative results, presented in table 1, show that our method achieved the highest performance, outperforming the second-best method (RIDCP) by 19.0%. Specifically, our method improved FADE, BRISQUE, and NIMA scores by 20.4%, 30.8%, and 7.0%, respectively. This demonstrates that our method surpasses current state-of-the-art techniques in both dehazing capability and the quality, and aesthetics of the generated images.

The visual comparisons of our proposed method and state-of-the-art algorithms are shown in figs. 4 and 5. We can observe that these methods have demonstrated some effectiveness in real-world dehazing tasks, but when images containing white objects, sky, or extreme haze, the results from PDN, DAD, PSD, and RIDCP exhibited varying degrees of dark patches and contrast inconsistencies. Conversely, D4 caused an overall reduction in brightness, leading to detail loss in darker areas. Under these conditions, DGUN produced relatively aesthetically pleasing results but lost significant local detail, impairing overall visual quality. Notably, PSD achieved higher brightness but suffered from severe oversaturation. CORUN+ consistently outperforms others by producing clearer images with natural colors and better contrast, effectively removing haze while preserving image details.

4.3 Ablation Study

Generalization and Effect of Colabator. We evaluate the performance and the impact of our proposed Colabator framework across different metrics. As shown in table 2, removing the fine-tuning phase of Colabator led to significant performance drops, highlighting its critical role in the dehazing process. To evaluate the generalizability of Colabator, we conducted additional experiments

| Dataset | PDN [57] | MBDN [10] | DH [13] | DAD [47] | PSD [6] | D4 [59] | RIDCP [54] | DGUN [37] | Ours |
|--------------|----------|-----------|---------|----------|---------|---------|-------------|-----------|-------------|
| RTTS[27] | 4.52 | 3.47 | 3.23 | 4.35 | 3.90 | 4.66 | 7.14 | 6.04 | 7.76 |
| Fattal’s[11] | 4.85 | 3.33 | 3.19 | 4.80 | 4.28 | 4.38 | 7.28 | 6.33 | 8.04 |

Table 5: User study scores on RTTS[27] and Fattal’s[11].

| Class(AP) | Hazy | PDN [57] | MBDN [10] | DH [13] | DAD [47] | PSD [6] | D4 [59] | RIDCP [54] | DGUN [37] | Ours |
|-----------|------|-------------|-----------|---------|----------|---------|---------|-------------|-------------|-------------|
| Bicycle | 0.51 | 0.55 | 0.54 | 0.47 | 0.52 | 0.52 | 0.54 | 0.57 | 0.55 | 0.59 |
| Bus | 0.25 | 0.29 | 0.27 | 0.23 | 0.29 | 0.25 | 0.28 | 0.32 | 0.31 | 0.31 |
| Car | 0.61 | 0.65 | 0.63 | 0.51 | 0.65 | 0.63 | 0.64 | 0.67 | 0.66 | 0.68 |
| Motor | 0.38 | 0.45 | 0.43 | 0.37 | 0.38 | 0.42 | 0.42 | 0.47 | 0.46 | 0.49 |
| Person | 0.73 | 0.76 | 0.75 | 0.69 | 0.74 | 0.74 | 0.75 | 0.76 | 0.76 | 0.77 |
| Mean | 0.50 | 0.54 | 0.52 | 0.45 | 0.52 | 0.51 | 0.53 | 0.56 | 0.55 | 0.57 |

Table 6: Object detection results on RTTS[27].

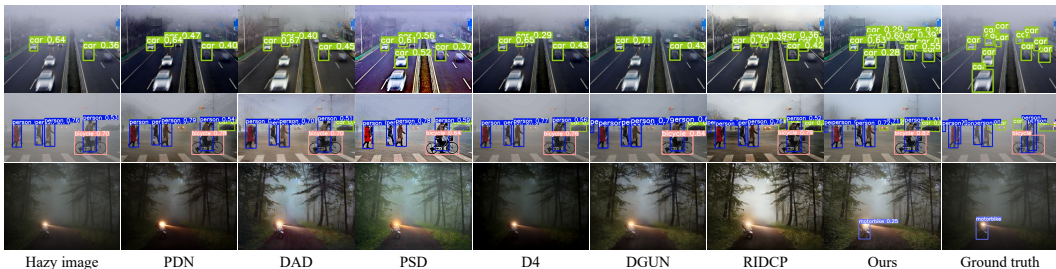


Figure 6: Visual comparison of object detection on RTTS [27].

by replacing our CORUN with the DGUN [37], while maintaining consistent training settings. Results in table 2 and fig. 1 indicate that Colaborator substantially enhances DGUN’s performance, demonstrating its effectiveness as a plug-and-play paradigm with strong generalization capabilities.

Effect of Colaborator. We validate the effect of our Colaborator. In table 3, we systematically removed critical components, such as iterative mean-teacher (IMD), trusted weighting, and the optimal label pool, from the model architecture. The outcomes indicate the performance deteriorates when these components are removed, highlighting their essential role in the system.

Ablations on stage number. The number of stages in a deep unfolding network significantly impacts its efficiency and performance. To investigate this, we experimented with different stage numbers for CORUN+, specifically choosing k values from the set $\{1, 2, 4, 6\}$. The results detailed in table 4, indicate that CORUN+ achieves high-quality dehazing with 4 stages. Notably, increasing the number of stages does not necessarily improve outcomes. Excessive stages can increase the network’s complexity, hinder convergence, and potentially introduce errors in the results.

4.4 User Study and Downstream Task

User Study. We conducted a user study to evaluate the human subjective visual perception of our proposed method against other methods. We invited five experts with an image processing background and 16 naive observers as testers. These testers were instructed to focus on three primary aspects: (i) Haze density compared to the original hazy image, (ii) Clarity of details in the dehazed image, and (iii) Color and aesthetic quality of the dehazed image. The results for each method, along with the corresponding hazy images, were presented to the testers anonymously. They scored each method on a scale from 1 (worst) to 10 (best). The hazy images were selected randomly, with a total of 225 images from RTTS[1] and 54 images from Fattal’s[11] dataset. The user study scores are reported in table 5, showing that our method achieved the highest average score.

Downstream Task Evaluation. The performance of high-level vision tasks, *e.g.* object detection and semantic segmentation, is greatly affected by image quality, with severely degraded images often leading to erroneous results [29, 51, 58]. To address this performance degradation, some methods have incorporated image restoration as a preprocessing step for high-level vision tasks. To validate the effectiveness of our approach for high-level vision, we utilized pretrained YOLOv3 [45], and tested it on the RTTS [27] dataset, and evaluated the results using the mean Average Precision (mAP) metric. As shown in table 6 and fig. 6, our method demonstrates a substantial advantage over existing methods, verifying our efficacy in facilitating high-level vision understanding.



Figure 7: Failure cases. Our results show low quality texture details.

4.5 Limitations and Future Work

In fig. 7, our CORUN+ model struggles to maintain result quality and preserve texture details when dealing with severely degraded inputs, such as strong compression and extreme high-density haze. This challenge persists across existing methods and remains unresolved. We attribute this difficulty to the model’s struggle in reconstructing scenes from dense fog, where information is often severely lacking or entirely lost, affecting the reconstruction of both haze-free and low haze density areas. Moreover, the model solely focuses on defogging and lacks the capability to address other image degradations, such as image deblurring[65] and low-light image enhancement [14], limiting its ability to achieve high-quality reconstruction results from complex degraded images. To address this limitation in future research, we propose not only focusing on environmental degradation but also considering additional information about image degradation when solving real-world dehazing problems. In addition to this, we can introduce more modalities as supplements to RGB images, enhancing the model’s ability to effectively recover details.

4.6 Broader Impacts

Real-world image dehazing is a crucial task in image restoration, aimed at removing haze degradation from images captured in real-world scenarios. In computer vision, dehazing can benefit downstream tasks such as object detection [66, 40, 41, 39], image segmentation [18, 19, 55, 17], and depth estimation [4, 26], with applications ranging from autonomous driving to security monitoring. Our paper introduces a cooperative unfolding network and a plug-and-play pseudo-labeling framework, achieving state-of-the-art performance in real-world dehazing tasks. Notably, image dehazing techniques have yet to exhibit negative social impacts. Our proposed CORUN and Colabator methods also do not present any foreseeable negative societal consequences.

5 Conclusions

In this paper, we introduce CORUN to cooperatively model atmospheric scattering and image scenes and thus incorporate physical information into deep networks. Furthermore, we propose Colabator, an iterative mean-teacher framework, to generate high-quality pseudo-labels by storing the best-ever results with global and local coherence in a dynamic label pool. Experiments demonstrate that our method achieves state-of-the-art performance in real-world image dehazing tasks, with Colabator also improving the generalization of other dehazing methods. The code will be released.

References

- [1] Bengio, Y., Léonard, N., Courville, A.: Estimating or propagating gradients through stochastic neurons for conditional computation. arXiv preprint arXiv:1308.3432 (2013) 9
- [2] Cai, Y., Lin, J., Lin, Z., Wang, H., Zhang, Y., Pfister, H., Timofte, R., Van Gool, L.: Mst++: Multi-stage spectral-wise transformer for efficient spectral reconstruction. In: Proceedings of the IEEE/CVF Conference on Computer Vision and Pattern Recognition. pp. 745–755 (2022) 4
- [3] Chen, C., Mo, J.: IQA-PyTorch: Pytorch toolbox for image quality assessment. [Online]. Available: <https://github.com/chaofengc/IQA-PyTorch> (2022) 8
- [4] Chen, S., Ye, T., Shi, J., Liu, Y., Jiang, J., Chen, E., Chen, P.: Dehrformer: Real-time transformer for depth estimation and haze removal from varicolored haze scenes. In: ICASSP 2023-2023 IEEE International Conference on Acoustics, Speech and Signal Processing (ICASSP). pp. 1–5. IEEE (2023) 10
- [5] Chen, X., Fan, Z., Li, P., Dai, L., Kong, C., Zheng, Z., Huang, Y., Li, Y.: Unpaired deep image dehazing using contrastive disentanglement learning. In: Avidan, S., Brostow, G., Cissé, M., Farinella, G.M., Hassner, T. (eds.) Computer Vision – ECCV 2022. pp. 632–648. Springer Nature Switzerland, Cham (2022) 2
- [6] Chen, Z., Wang, Y., Yang, Y., Liu, D.: Psd: Principled synthetic-to-real dehazing guided by physical priors. In: Proceedings of the IEEE/CVF Conference on Computer Vision and Pattern Recognition (CVPR). pp. 7180–7189 (2021) 2, 3, 7, 8, 9
- [7] Choi, L.K., You, J., Bovik, A.C.: Referenceless prediction of perceptual fog density and perceptual image defogging. IEEE Transactions on Image Processing (TIP) 24(11), 3888–3901 (2015) 7
- [8] Cong, X., Gui, J., Zhang, J., Hou, J., Shen, H.: A semi-supervised nighttime dehazing baseline with spatial-frequency aware and realistic brightness constraint (2024) 3
- [9] Diederik, P.K.: Adam: A method for stochastic optimization. (No Title) (2014) 7
- [10] Dong, H., Pan, J., Xiang, L., Hu, Z., Zhang, X., Wang, F., Yang, M.H.: Multi-scale boosted dehazing network with dense feature fusion. In: Proceedings of the IEEE/CVF Conference on Computer Vision and Pattern Recognition (CVPR). pp. 2157–2167 (2020) 2, 7, 8, 9
- [11] Fattal, R.: Dehazing using color-lines. ACM transactions on graphics (TOG) 34(1), 1–14 (2014) 7, 8, 9
- [12] Goodfellow, I.J., Pouget-Abadie, J., Mirza, M., Xu, B., Warde-Farley, D., Ozair, S., Courville, A.C., Bengio, Y.: Generative adversarial nets. In: Neural Information Processing Systems (NeruIPS) (2014) 3
- [13] Guo, C.L., Yan, Q., Anwar, S., Cong, R., Ren, W., Li, C.: Image dehazing transformer with transmission-aware 3d position embedding. In: Proceedings of the IEEE/CVF Conference on Computer Vision and Pattern Recognition (CVPR). pp. 5812–5820 (2022) 2, 7, 8, 9
- [14] He, C., Fang, C., Zhang, Y., Li, K., Tang, L., You, C., Xiao, F., Guo, Z., Li, X.: Reti-diff: Illumination degradation image restoration with retinex-based latent diffusion model. arXiv preprint arXiv:2311.11638 (2023) 10
- [15] He, C., Li, K., Xu, G., Yan, J., Tang, L.: Hqg-net: Unpaired medical image enhancement with high-quality guidance. IEEE Trans. Neural Netw. Learn. Syst. (2023) 1
- [16] He, C., Li, K., Xu, G., Zhang, Y., Hu, R., Guo, Z., Li, X.: Degradation-resistant unfolding network for heterogeneous image fusion. In: ICCV. pp. 12611–12621 (2023) 2
- [17] He, C., Li, K., Zhang, Y., Tang, L., Zhang, Y., Guo, Z., Li, X.: Camouflaged object detection with feature decomposition and edge reconstruction. In: CVPR. pp. 22046–22055 (2023) 10
- [18] He, C., Li, K., Zhang, Y., Xu, G., Tang, L.: Weakly-supervised concealed object segmentation with sam-based pseudo labeling and multi-scale feature grouping. NeurIPS (2024) 10

- [19] He, C., Li, K., Zhang, Y., Zhang, Y., Guo, Z., Li, X.: Strategic preys make acute predators: Enhancing camouflaged object detectors by generating camouflaged objects. In: ICLR (2024) [10](#)
- [20] He, K., Sun, J., Tang, X.: Single image haze removal using dark channel prior. IEEE Transactions on Pattern Analysis and Machine Intelligence (TPAMI) **33**(12), 2341–2353 (2010) [2](#)
- [21] He, M., Hui, L., Bian, Y., Ren, J., Xie, J., Yang, J.: Ra-depth: Resolution adaptive self-supervised monocular depth estimation. In: European Conference on Computer Vision. pp. 565–581. Springer (2022) [7](#)
- [22] He, R., Zheng, W.S., Tan, T., Sun, Z.: Half-quadratic-based iterative minimization for robust sparse representation. IEEE transactions on pattern analysis and machine intelligence **36**(2), 261–275 (2013) [3](#)
- [23] Ju, M., He, C., Liu, J.: Ivf-net: An infrared and visible data fusion deep network for traffic object enhancement in intelligent transportation systems. IEEE Trans. Intell. Transp. Syst. (2022) [3](#)
- [24] Ju, M., Zhang, D., Wang, X.: Single image dehazing via an improved atmospheric scattering model. The Visual Computer **33**, 1613–1625 (2017) [2](#)
- [25] Ke, J., Wang, Q., Wang, Y., Milanfar, P., Yang, F.: Musiq: Multi-scale image quality transformer. In: Proceedings of the IEEE/CVF international conference on computer vision. pp. 5148–5157 (2021) [7](#)
- [26] Lee, B.U., Lee, K., Oh, J., Kweon, I.S.: Cnn-based simultaneous dehazing and depth estimation. In: 2020 IEEE International Conference on Robotics and Automation (ICRA). pp. 9722–9728. IEEE (2020) [10](#)
- [27] Li, B., Ren, W., Fu, D., Tao, D., Feng, D., Zeng, W., Wang, Z.: Benchmarking single-image dehazing and beyond. IEEE Transactions on Image Processing **28**(1), 492–505 (2019) [7](#), [8](#), [9](#)
- [28] Li, M., Fu, Y., Liu, J., Zhang, Y.: Pixel adaptive deep unfolding transformer for hyperspectral image reconstruction. In: Proceedings of the IEEE/CVF International Conference on Computer Vision. pp. 12959–12968 (2023) [3](#)
- [29] Li, S., Araujo, I.B., Ren, W., Wang, Z., Tokuda, E.K., Junior, R.H., Cesar-Junior, R., Zhang, J., Guo, X., Cao, X.: Single image deraining: A comprehensive benchmark analysis. In: Proceedings of the IEEE/CVF Conference on Computer Vision and Pattern Recognition. pp. 3838–3847 (2019) [9](#)
- [30] Li, Y., Chang, Y., Gao, Y., Yu, C., Yan, L.: Physically disentangled intra-and inter-domain adaptation for varicolored haze removal. In: Proceedings of the IEEE/CVF Conference on Computer Vision and Pattern Recognition. pp. 5841–5850 (2022) [2](#)
- [31] Liu, X., Ma, Y., Shi, Z., Chen, J.: Griddehazenet: Attention-based multi-scale network for image dehazing. In: Proceedings of the IEEE International Conference on Computer Vision (ICCV). pp. 7314–7323 (2019) [2](#)
- [32] Liu, Y., Yan, Z., Chen, S., Ye, T., Ren, W., Chen, E.: Nighthazeformer: Single nighttime haze removal using prior query transformer. p. 4119–4128. MM '23, Association for Computing Machinery, New York, NY, USA (2023) [3](#)
- [33] Loshchilov, I., Hutter, F.: Sgdr: Stochastic gradient descent with warm restarts. arXiv preprint arXiv:1608.03983 (2016) [7](#)
- [34] Loshchilov, I., Hutter, F.: Decoupled weight decay regularization. arXiv preprint arXiv:1711.05101 (2017) [7](#)
- [35] Luo, Z., Gustafsson, F.K., Zhao, Z., Sjölund, J., Schön, T.B.: Controlling vision-language models for universal image restoration. arXiv preprint arXiv:2310.01018 (2023) [7](#)
- [36] Mittal, A., Moorthy, A.K., Bovik, A.C.: No-reference image quality assessment in the spatial domain. IEEE Transactions on image processing **21**(12), 4695–4708 (2012) [8](#)

- [37] Mou, C., Wang, Q., Zhang, J.: Deep generalized unfolding networks for image restoration. In: Proceedings of the IEEE/CVF Conference on Computer Vision and Pattern Recognition. pp. 17399–17410 (2022) [2](#), [3](#), [7](#), [8](#), [9](#)
- [38] Paszke, A., Gross, S., Massa, F., Lerer, A., Bradbury, J., Chanan, G., Killeen, T., Lin, Z., Gimelshein, N., Antiga, L., et al.: Pytorch: An imperative style, high-performance deep learning library. *Advances in neural information processing systems* **32** (2019) [7](#)
- [39] Pu, Y., Han, Y., Wang, Y., Feng, J., Deng, C., Huang, G.: Fine-grained recognition with learnable semantic data augmentation. *IEEE Transactions on Image Processing* (2024) [10](#)
- [40] Pu, Y., Liang, W., Hao, Y., Yuan, Y., Yang, Y., Zhang, C., Hu, H., Huang, G.: Rank-detr for high quality object detection. *Advances in Neural Information Processing Systems* **36** (2024) [10](#)
- [41] Pu, Y., Wang, Y., Xia, Z., Han, Y., Wang, Y., Gan, W., Wang, Z., Song, S., Huang, G.: Adaptive rotated convolution for rotated object detection. In: Proceedings of the IEEE/CVF International Conference on Computer Vision. pp. 6589–6600 (2023) [10](#)
- [42] Qin, X., Wang, Z., Bai, Y., Xie, X., Jia, H.: Ffa-net: Feature fusion attention network for single image dehazing. *Proceedings of the AAAI Conference on Artificial Intelligence* **34**(07) (2020) [2](#)
- [43] Qiu, Y., Zhang, K., Wang, C., Luo, W., Li, H., Jin, Z.: Mb-taylorformer: Multi-branch efficient transformer expanded by taylor formula for image dehazing. In: Proceedings of the IEEE/CVF International Conference on Computer Vision. pp. 12802–12813 (2023) [2](#)
- [44] Radford, A., Kim, J.W., Hallacy, C., Ramesh, A., Goh, G., Agarwal, S., Sastry, G., Askell, A., Mishkin, P., Clark, J., et al.: Learning transferable visual models from natural language supervision. In: International conference on machine learning. pp. 8748–8763. PMLR (2021) [5](#)
- [45] Redmon, J., Farhadi, A.: Yolov3: An incremental improvement. *arXiv preprint arXiv:1804.02767* (2018) [9](#)
- [46] Sakaridis, C., Dai, D., Hecker, S., Van Gool, L.: Model adaptation with synthetic and real data for semantic dense foggy scene understanding. In: Proceedings of the European Conference on Computer Vision (ECCV). pp. 687–704 (2018) [1](#)
- [47] Shao, Y., Li, L., Ren, W., Gao, C., Sang, N.: Domain adaptation for image dehazing. In: Proceedings of the IEEE/CVF Conference on Computer Vision and Pattern Recognition (CVPR). pp. 2808–2817 (2020) [2](#), [7](#), [8](#), [9](#)
- [48] Simonyan, K., Zisserman, A.: Very deep convolutional networks for large-scale image recognition. In: Bengio, Y., LeCun, Y. (eds.) International Conference on Learning Representations (ICLR) (2015), <http://dblp.uni-trier.de/db/conf/iclr/iclr2015.html#SimonyanZ14a> [6](#)
- [49] Talebi, H., Milanfar, P.: Nima: Neural image assessment. *IEEE Transactions on Image Processing (TIP)* **27**(8), 3998–4011 (2018) [8](#)
- [50] Tong, M., Wang, Y., Cui, P., Yan, X., Wei, M.: Semi-uforformer: Semi-supervised uncertainty-aware transformer for image dehazing (2022) [3](#)
- [51] VidalMata, R.G., Banerjee, S., RichardWebster, B., Albright, M., Davalos, P., McCloskey, S., Miller, B., Tambo, A., Ghosh, S., Nagesh, S., et al.: Bridging the gap between computational photography and visual recognition. *IEEE transactions on pattern analysis and machine intelligence* **43**(12), 4272–4290 (2020) [9](#)
- [52] Wang, J., Wu, S., Yuan, Z., Tong, Q., Xu, K.: Frequency compensated diffusion model for real-scene dehazing. *Neural Networks* **175**, 106281 (2024) [2](#)
- [53] Wu, H., Qu, Y., Lin, S., Zhou, J., Qiao, R., Zhang, Z., Xie, Y., Ma, L.: Contrastive learning for compact single image dehazing. In: Proceedings of the IEEE/CVF conference on computer vision and pattern recognition. pp. 10551–10560 (2021) [2](#)

- [54] Wu, R., Duan, Z., Guo, C., Chai, Z., Li, C.: Ridcp: Revitalizing real image dehazing via high-quality codebook priors. In: Proceedings of the IEEE/CVF Conference on Computer Vision and Pattern Recognition (2023) [2](#), [7](#), [8](#), [9](#)
- [55] Xiao, F., Zhang, P., He, C., Hu, R., Liu, Y.: Concealed object segmentation with hierarchical coherence modeling. In: CAAI. pp. 16–27. Springer (2023) [10](#)
- [56] Xu, G., He, C., Wang, H., Zhu, H., Ding, W.: Dm-fusion: Deep model-driven network for heterogeneous image fusion. *IEEE Trans. Neural Netw. Learn. Syst.* (2023) [2](#)
- [57] Yang, D., Sun, J.: Proximal dehaze-net: A prior learning-based deep network for single image dehazing. In: Proceedings of the european conference on computer vision (ECCV). pp. 702–717 (2018) [2](#), [3](#), [7](#), [8](#), [9](#)
- [58] Yang, W., Yuan, Y., Ren, W., Liu, J., Scheirer, W.J., Wang, Z., Zhang, T., Zhong, Q., Xie, D., Pu, S., et al.: Advancing image understanding in poor visibility environments: A collective benchmark study. *IEEE Transactions on Image Processing* **29**, 5737–5752 (2020) [9](#)
- [59] Yang, Y., Wang, C., Liu, R., Zhang, L., Guo, X., Tao, D.: Self-augmented unpaired image dehazing via density and depth decomposition. In: Proceedings of the IEEE/CVF Conference on Computer Vision and Pattern Recognition (CVPR). pp. 2037–2046 (2022) [2](#), [7](#), [8](#), [9](#)
- [60] Ye, T., Jiang, M., Zhang, Y., Chen, L., Chen, E., Chen, P., Lu, Z.: Perceiving and modeling density is all you need for image dehazing. arXiv preprint arXiv:2111.09733 (2021) [2](#)
- [61] You, D., Xie, J., Zhang, J.: Ista-net++: Flexible deep unfolding network for compressive sensing. In: 2021 IEEE International Conference on Multimedia and Expo (ICME). pp. 1–6. IEEE (2021) [3](#)
- [62] Zhang, J., Ghanem, B.: Ista-net: Interpretable optimization-inspired deep network for image compressive sensing. In: Proceedings of the IEEE conference on computer vision and pattern recognition. pp. 1828–1837 (2018) [3](#)
- [63] Zhang, K., Gool, L.V., Timofte, R.: Deep unfolding network for image super-resolution. In: Proceedings of the IEEE/CVF conference on computer vision and pattern recognition. pp. 3217–3226 (2020) [3](#)
- [64] Zhang, Y., Zhou, S., Li, H.: Depth information assisted collaborative mutual promotion network for single image dehazing. arXiv preprint arXiv:2403.01105 (2024) [2](#)
- [65] Zhang, Y., Zheng, P., Yan, W., Fang, C., Cheng, S.S.: A unified framework for microscopy defocus deblur with multi-pyramid transformer and contrastive learning. In: Proceedings of the IEEE/CVF Conference on Computer Vision and Pattern Recognition (CVPR). pp. 11125–11136 (June 2024) [10](#)
- [66] Zhang, Z., Zhao, L., Liu, Y., Zhang, S., Yang, J.: Unified density-aware image dehazing and object detection in real-world hazy scenes. In: Proceedings of the Asian Conference on Computer Vision (2020) [10](#)
- [67] Zheng, Y., Zhan, J., He, S., Dong, J., Du, Y.: Curricular contrastive regularization for physics-aware single image dehazing. In: Proceedings of the IEEE/CVF conference on computer vision and pattern recognition. pp. 5785–5794 (2023) [2](#)
- [68] Zhou, M., Huang, J., Zheng, N., Li, C.: Learned image reasoning prior penetrates deep unfolding network for panchromatic and multi-spectral image fusion. In: Proceedings of the IEEE/CVF International Conference on Computer Vision. pp. 12398–12407 (2023) [3](#)
- [69] Zhu, J.Y., Park, T., Isola, P., Efros, A.A.: Unpaired image-to-image translation using cycle-consistent adversarial networks. In: Computer Vision (ICCV), 2017 IEEE International Conference on (2017) [2](#)